DOI: 10.1002/ ((please add manuscript number))
Article type: Full Paper

Design of lanthanide-based OLEDs with remarkable circularly polarized electroluminescence

Francesco Zinna[a], *Mariacecilia Pasini*[b], *Francesco Galeotti*[b], *Chiara Botta*[b], *Lorenzo Di Bari*[a,*] *and Umberto Giovanella*[b,*]

F. Zinna, Prof. L. Di Bari
Dipartimento di Chimica e Chimica Industriale, Università di Pisa, via Moruzzi 13, I-56124 Pisa, Italy
E-mail: lorenzo.dibari@unipi.it
M. Pasini, F. Galeotti, C. Botta, U. Giovanella
Istituto per lo Studio delle Macromolecole (ISMAC), CNR, Via A. Corti 12, 20133 , Milano, Italy
Email: u.giovanella@ismac.cnr.it

Keywords: lanthanides, OLEDs, circular polarization, chiral electroluminescence, interfacial layers

Abstract

OLEDs able to directly emit circularly polarized (CP) electroluminescence (CP-OLEDs) are rapidly gaining much interest, due to their possible applications in displays with anti-glare filters and 3D displays. Development of more efficient CP-OLEDs could open the way to their use as a source of CP light in point-of-care andpersonalized diagnostic tools, since CP light alteration could be related to health state of illuminated tissues.
Chiral lanthanide complexes can be employed efficiently in obtaining highly circularly polarized emission. In this work we show that their efficiency can be improved both in terms of EQE (measured on all the Eu bands) and polarization (as measured by g_{EL}), by using new electrode interlayers and through a fine tuning of the architecture of the device. In this way, we obtain polarization performances (g_{EL} up to 1) about 3 times higher than for any other CP-OLED reported so far. Moreover, we identify the main factors affecting polarization inside such devices. For the first time, we show that the position of the recombination zone plays a major role on the polarization outcomes. Indeed by using a cathode injecting layer, which promotes electron injection, the RZ is displaced toward the cathode resulting in higher polarization. In order to rationalize these results, for the first time, we developed a model relating the g_{EL} factor of the device with the position of the recombination zone allied with the reflection on the cathode. The values predicted by our model are in qualitative agreement with the experimental ones.
These results contribute to elucidate some of the aspects to take into account when developing CP-OLEDs suitable to switch to practical applications.

1. Introduction

Linearly (LP) and circularly polarized (CP) organic light-emitting diodes (CP-OLEDs) are an innovative and emerging technology. The first and possibly most natural application for CP-OLEDs is in displays where polarized light is used and manipulated to prevent reflection of ambient light and achieve high contrast three-dimensional (3-D) images and true black. [J. Am. Chem. Soc., 2016, 138 (31), pp 9743] Moreover a CP screen reduces the perceived distortion found at some angles when the display is viewed through a LP filter, like polarized sunglasses, allowing for enhanced outdoor viewing of laptops or smartphones. Even more importantly, non-invasive and real-time polarized optical techniques are becoming increasingly popular in the field of biomedical diagnosis and care {Tuchin, 2002 #17;Tuchin, 2006 #18}. In this context, red and near infrared radiation is particularly useful, given its ability to penetrate organic tissues {Moreira, 2011 #291}. Furthermore, biological molecules interact with polarized light, whose alteration through scattering, refraction or absorption could be related to the composition or health state of the illuminated tissue {Sparks, 2009 #31;Kunnen, 2015 #28}.

Unfortunately, LP light quickly loses its polarization due to multiple scattering in turbid media (depending on size and shape of scattering particles) thus limiting its practical application mostly to probe surface tissues, whereas CP light can maintain its polarization longer than LP one {Tuchin, 2006 #18}.

The manufacture of compact and portable point-of-care medical systems, based on CP technology, uncoupled from centralized laboratories would be cost-effective and time-saving, with several advantages including broader accessibility to health care worldwide. However, usage of conventional optical systems to generate CP light involves multiple optical elements, making it challenging to realize small, cheap and integrated devices for portable point-of-care testing. Recently, very advanced compact optical elements for manipulation of CP light were

reported and validated in laboratory including sources {Zhang, 2014 #21}, quarter waveplates {Yu, 2012 #23}, polarizers {Gansel, 2009 #24} and beam splitters {Turner, 2013 #25}.

On the other hand, organic optoelectronic devices, like OLEDs, could be a valuable alternative, since they combine unique advantages of lightness as well as portability, wearability and battery saving, with the management of color and power of radiation emitted. Introducing CP-OLEDs as light source, possibly in combination with a chiral detection systems, could have a significant medical and social impact, as it would open up new perspectives in the application of CP light in the field of innovative portable devices such as smart bandage or diagnostic tools, suited also in poorly resourced environments.

So far, CP-OLEDs technology have relied mostly on conjugated polymers able to emit CP electroluminescence (EL) once aggregated in supramolecular chiral structures. Such supramolecular chirality may be determined either by the intrinsic chirality carried by the polymer itself {Oda, 2000 #13;Peeters, 1997 #12;Geng, 2003 #14}or by introducing chiral dopants {Yang, 2013 #10;Feuillastre, 2016 #32;Roose, 2016 #465}. The polarization degree[in nota: Here we follow the convention used in chiroptical spectroscopy: right polarized light is defined as the point of the electric field vector **E** of the electromagnetic wave describing a right-handed screw ref. L. D. Barron Molecular Light Scattering and Optical Activity 2nd edition Cambridge University Press, 2004] of CP-OLEDs, measured in terms of the EL dissymmetry factor $g_{EL} = 2(I_L - I_R)/(I_L + I_R)$, where I_L and I_R are the intensities of the left and right polarized component of the emission, remains fairly low (< |0.2|). Recently we proposed an alternative approach {Zinna, 2015 #11} based on single chiral small molecules (such as lanthanide complexes) able to emit intrinsic highly CP EL, without relying on supramolecular properties which dramatically depend on the preparation process {Craig, 2003 #370}. Similarly, Zuo et al.{Li, 2015 #324} employed chiral Iridium complexes as dopant emitters in vacuum processed devices, with rather low g_{EL}s (in the order of 10^{-3}). More recently, Brandt et al. [J. Am. Chem. Soc., 2016, 138 (31), pp 9743] used a helicene-Pt

complex[Shen, C.; Anger, E.; Srebro, M.; Vanthuyne, N.; Deol, K. K.; Jefferson, T. D.; Muller, G.; Williams, J. A. G.; Toupet, L.; Roussel, C.; Autschbach, J.; Reau, R.; Crassous, J. *Chem. Sci.* **2014**, *5*, 1915–1927.] reaching g_{EL}= 0.35 through Pt-centered phosphorescence. Our own proof-of-concept device based on a chiral europium complex emitter, reached the highest reported g_{EL} value for any CP-OLED close to |0.8| at 595 nm {Zinna, 2015 #11}. The advantages of our design consist in i) pure red color, typical of sharp emission lines of Eu(III) complexes leading in principle to highly saturated colors (J. Andres, et al, *Adv. Funct. Mater.*, **2014**, *24*, 5029.) needed e.g. in electronic displays; ii) the use of chiral ligands easy accessible, either commercially or prepared {Zinna, 2015 #313} from inexpensive products available in the natural chiral pool; iii) the use of a well-established device architecture based on solution processable active layer; iv) the possibility to transfer the same technology to other Ln(III) emitters to cover different spectral regions, including the near infrared one.

We should point out that in such devices usually two bands with opposite polarization are usually observed; in order to switch to practical applications these two bands can be separated using high-pass or low-pass filters. For more futuristic applications, such as in CP-OLED smart bandage, it would be conceivable to use polarization-sensitive detection systems (Yang, et al. *Nature Photonics* 2013, 7, 634) responsive to different wavelengths, in this way the change in light polarization would be monitored on both left and right handed CP light simultaneously.

In this exciting scenario, we develop a second-generation Ln-based CP-OLEDs with very high intrinsic CP red emission, outperforming our own previous results {Zinna, 2015 #11}. By the judicious use of electrode interlayers, the CP-OLEDs presented here attain the unprecedented polarization of emitted photons at 595 nm (65-75% polarization) and an optimized device displays external quantum efficiencies (EQE) enhanced by one order of magnitude with respect to our earlier proof-of-concept achievement. Moreover, we identify for the first time to the best of our knowledge, the main factors affecting CP-OLEDs

performance by combining experimental data and modeling, to assist one optimizing total emission and circular polarization of a device. Our long term goal is to bring the technology of CP-OLEDs to the next technology readiness level (or TRL).

2. Results and discussion

We turned our attention to β-diketonate ligands since they are very good sensitizers for Eu ion and photoluminescence (PL) quantum yield (PLQY) can exceed 50 % in solution {Freund, 2011 #33} and 80 % in powder {Malta, 1998 #308}. When the β-dicarbonyl motif is linked to a chiral framework, high levels of CP emission can be achieved, although the development of emitters with both significant PLQY and g_{PL} is still an expectation.

The chiral complex $CsEu(hfbc)_4$ (hfbc = 3-heptafluorobutyryl camphorate, **Figure 1**) with the highest known CP photoluminescence (PL) (g_{PL} = 1.38 at 595 nm, meaning a I_L/I_R ratio of 85:15; g_{PL} is defined in analogy to g_{EL}) {Lunkley, 2011 #30} is used as the chiral emitter. Despite its low PLQY (3.5 % in solution and ~3 % in powder, Table S1) which limits the efficiency of the devices, $CsEu(hfbc)_4$ highly polarized emission is very convenient for identifying key factors that affect circular polarization in CP-OLEDs. Recently, Yuasa et al. reported that the photophysical properties of $CsEu(hfbc)_4$ (g_{EL} and PLQY) can be improved in solid state thanks to specific packing and aggregation modes.[Chem. Commun., 2016, 52, 9885-9888, DOI: 10.1039/C6CC05022K]

For a correct operation in a solution processed OLED, the β-diketonate Eu(III)-complex must necessarily be homogeneously dispersed in a semiconducting conjugated matrix (so called host/guest approach) {Zhang, 2012 #46;Freund, 2011 #33} that features a sufficiently high triplet energy (E_T) to prevent energy back transfer {Freund, 2011 #33}, a suitable HOMO/LUMO energy levels to confine radiative excitons on the guest sites, and a bipolar

charge transport. The matrix plays an even more crucial role in CP-OLEDs behavior since its emission can be broad and it is certainly not polarized, which is an issue for both color purity and polarization performance (g_{EL}) of the device. Hence, the selection of a good compound as host and the optimal blend formulation to address at the same time all those issues is very challenging.

Our earlier results showed that polyvinylcarbazole (PVK, Figure 1) is a suitable host for $CsEu(hfbc)_4$ complex to achieve Eu-centered EL with large g_{EL} {Zinna, 2015 #11}. However, the difference between g_{PL} and g_{EL} was significant, indicating that there is still room for improvement in polarization performances.

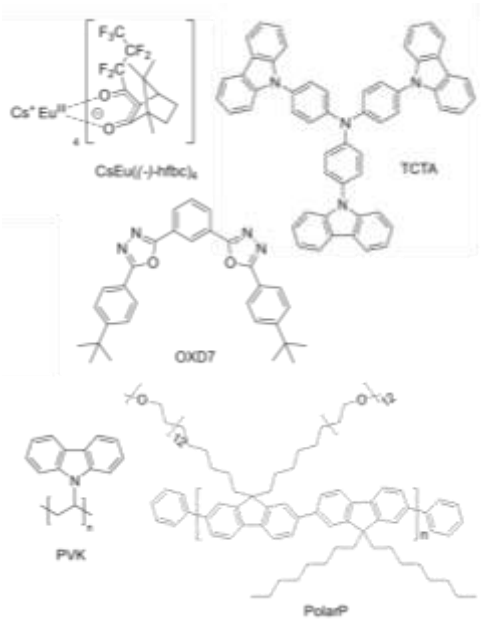

Figure 1. (a) Chemical structures of the $CsEu((–)\text{-hfbc})_4$, TCTA and OXD7 compounds. The chemical structures of PVK and PolarP used as interfacial layer (IL) are also shown.

The commercially available tris(4-carbazoyl-9-ylphenyl)amine (hereafter TCTA, Figure 1) is here proposed as an alternative to PVK in solution-processed CP-OLEDs, since its UV emission is spectrally more separated from Eu(III) complex emission with respect to PVK. This would be beneficial for higher polarization degree since the emission from the polymeric host is not polarized and its contribution would decrease the polarization (in terms of g_{EL}

factor) of the device in the case of overlap with the polarized Eu-centered bands. E_T of TCTA (2.8 eV, table S2) is high enough with respect to CsEu(*(–)*-hfbc)$_4$ one (2.45 eV, Figure S2) to avoid energy back transfer. The electron transporting 1,3-Bis[2-(4-tert -butylphenyl)-1,3,4-oxadiazo-5-yl]benzene (OXD7, Figure 1) is added to the blend to achieve bipolar charge transport [inserire manualmente il REF: TCTA and OXD-7 have been used as hole- and electron transport materials for a long time because they possess relatively high hole and electron mobility of ~10^{-4} and ~10^{-5} cm^2/Vs].

The CsEu(*(–)*-hfbc)$_4$ complex is dispersed in TCTA:OXD7 (1:1 wt.) in 12 wt.% mass ratio and the mixture is dissolved in $CHCl_3$ (15 mg/mL). The present study is conducted only on the enantiomer CsEu(*(–)*-hfbc)$_4$ as we demonstrated previously that the behavior of the two enantiomers is identical (*viz*. opposite) within the experimental error, as expected {Zinna, 2015 #11}.

The absorption spectrum (**Figure 2**a) is dominated by the host matrix with a main peak at 295 nm and shoulders at 320, 330 and 350 nm, and the absorption band of CsEu(*(–)*-hfbc)$_4$ lies beneath, with a peak at 310 nm. Films are highly transparent (transmittance, T > 96 %) in the visible range 400-700 nm (Figure S3). Once excited at 330 nm, the PL spectrum features the desired red emission with typical Eu(III) transitions and an UV contribution (peak at 369 nm) from the matrix (Figure 2b). The spectral overlap between host emission and Eu(III) complex absorption (Figure 2c) enables a long-range resonant energy transfer (FRET) from the matrix to the CsEu(*(–)*-hfbc)$_4$ complex. In fact, the PL excitation spectrum (PLE, Figure 2c) of TCTA:OXD7:12wt.% CsEu(*(–)*-hfbc)$_4$ film monitored at 612 nm (Eu-complex hypersensitive transition) shows contribution of both OXD7 and TCTA. The electronic circular dichroism (ECD) signal of the blend film (Figure 2d) is identical in shape to the spectrum of the complex in solution (Figure S4). This is a strong indication that the chiral Eu complex in the active layer has the same structure as the one studied in solution. The CP PL of the blend film (Figure 2e) displays g_{PL} values of -1.21±0.02 and 0.16±0.02 for 595 nm

($^5D_0 \rightarrow {}^7F_1$) and 612 nm ($^5D_0 \rightarrow {}^7F_2$) transitions respectively. These values are only slightly lower than CsEu(hfbc)$_4$ in solution, meaning that the TCTA:OXD7 matrix has little influence on the intrinsic polarization of the complex. Spin-coated films are homogeneous and very flat with root mean square roughness of 0.22 nm (Figure 2f).

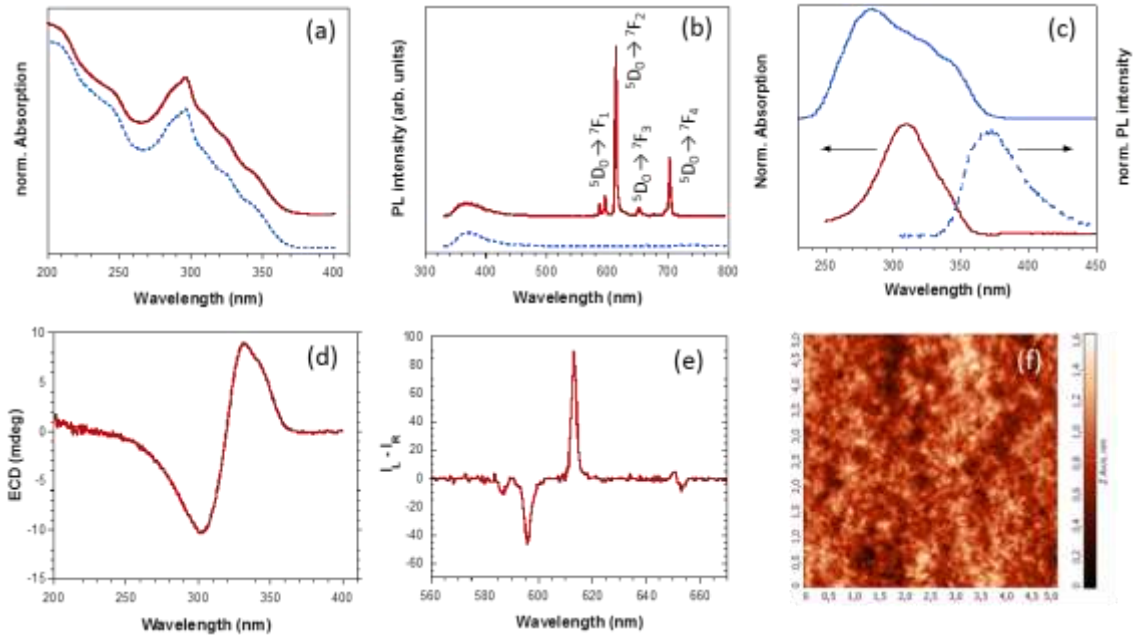

Figure 2. (a) Normalized absorbance and (b) PL spectra of TCTA:OXD7 (blue dotted line) and TCTA:OXD7:CsEu(*(–)*-hfbc)$_4$ (red solid line, vertically shifted for clarity) films excited at 330 nm; (c) normalized absorption of CsEu(*(–)*-hfbc)$_4$ solution (red solid line), PL spectrum of TCTA:OXD7 film (blue dotted line) and PLE of TCTA:OXD7:CsEu(*(–)*-hfbc)$_4$ film (blue solid line); (d) ECD and (e) CP PL spectrum of TCTA:OXD7:CsEu(*(–)*-hfbc)$_4$ film; (f) AFM tapping mode 5 x μm 5 μm image of TCTA:OXD7:CsEu(*(–)*-hfbc)$_4$ film.

On the basis of this optimal blend formulation, we manufactured CP-OLEDs with the architecture ITO/PEDOT:PSS/TCTA:OXD7:CsEu(*(–)*-hfbc)$_4$ (12 wt.%)/Ba/Al (**Figure 3**a). The thickness (d) of the active layer affects g_{EL} (Figure S5), thus it is fixed at 75±5 nm since this showed the best performance in PVK-based devices {Zinna, 2015 #11}.

The Ba/Al layer used as a cathode in OLEDs is typically thick (d > 100 nm) in order to reflect all the radiation back to the transparent glass substrate, but the reflection of the emitted light is a major issue for the polarization performance of the CP-OLEDs. The origin of this drawback

stems from a fundamental physical reason: the handedness of CP light is reversed upon reflection, therefore the degree of polarization, measured for the light exiting the transparent anode window, decreases as an effect of the reflection on the mirrored cathode{Zinna, 2015 #11}. To quantify the effect of reflection at the cathode on the PL polarization, we cover the blend film with 100 nm thick Al film and measure the CP PL by exciting and collecting light from the glass side (back scattering configuration). The g_{PL} values are lowered to -0.11±0.01 (from -1.21 in the uncovered film) at 595 nm and below the experimental error at 612 nm.

In CP-OLEDs, the dependence of g_{EL} on cathode transparency, hence on its reflectivity, is also investigated and compared to the results achieved earlier with PVK as a host. A film of 4 nm of Ba is deposited by thermal evaporation in high vacuum ad successively covered by 6 nm (device A), 20 nm (device B) or 110 nm (device C) of Al layer (**Figure 3**a). Accordingly, the cathode transmittance, T, ranges from 50 % to ~ 0 %. The EL spectra for all the devices show pure Eu-centered emission, with main typical transitions $^5D_0 \rightarrow {}^7F_1$ (595 nm), the hypersensitive $^5D_0 \rightarrow {}^7F_2$ (612 nm), $^5D_0 \rightarrow {}^7F_3$ (around 635 nm), and $^5D_0 \rightarrow {}^7F_4$ (around 685 nm) (Figure 3c). The CP EL is measured by following the method reported earlier {Zinna, 2015 #11}.

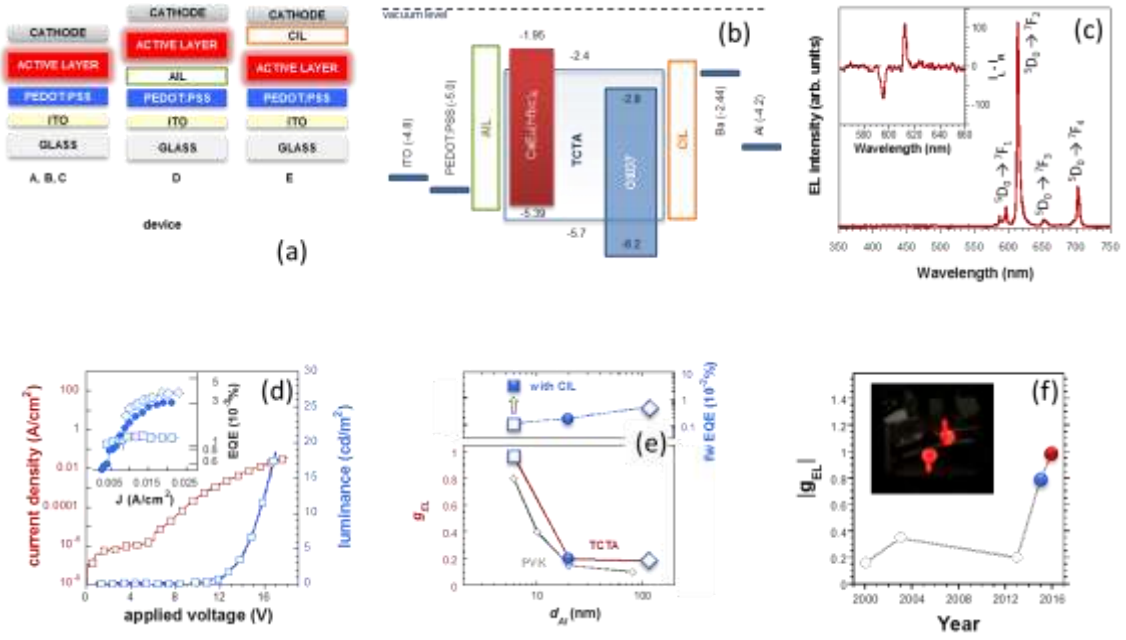

Figure 3. (a) Investigated CP-OLED architectures: single layer with 6 nm (A), 20 nm (B) and 110 nm (C) Al thickness, with AIL (D) and CIL (E) charge regulating layers; (b) flat band energy level diagram of all CP-OLEDs constituent layers; (c) representative EL spectra of CP-OLED featuring typical Eu(III) complex transitions and (inset) CP EL of the device A; (d) representative JLV characteristic curves of device A and (inset) EQE recorded in forward (fw) direction (glass side) for the devices A (□), B (●), C (◇); (e) g_{EL} (measured at 595 nm) and EQE of devices A (□), B (●), C (◇), E (■) versus Al layer thickness; g_{EL} (595 nm) (◇) behavior of ITO/PEDOT:PSS/PVK:OXD7:CsEu(*(–)*-hfbc)$_4$/Ba/Al is reported for comparison; (f) chronologic evolution of g_{EL} values of CP-OLEDs: state-of-the-art (●) {Zinna, 2015 #11} and present work (●); inset, image of working CP-OLEDs prototype.

For the semitransparent Al layer (device A, d_{Al} = 6 nm) we measure a remarkable g_{EL} = -1.00±0.08 at 595 nm and 0.19±0.08 at 612 nm (**Table 1**). This outstanding result outperforms the state-of-the-art CP-OLEDs {Zinna, 2015 #11}, with about 75% of the emitted photons at 595 nm circularly polarized (Figure 2f). For a less transparent cathode (device B, d_{Al} = 20 nm), the g_{EL} drops to -0.21±0.06 and -0.03±0.01 at 595 nm and 612 nm respectively, which is slightly higher than in the case of PVK host. For a cathode with the maximum reflection (device C, d_{Al} > 100 nm), the g_{EL} is further reduced to -0.15±0.06 at 595 nm and 0.03±0.01 at 612 nm, in agreement, in the range of experimental error, with the values of g_{PL} of Al-covered blend film (Table 1).

Table 1. PL and EL dissymmetry factors (g_{PL} and g_{EL}) for CsEu((-)-hfbc)$_4$ dispersed in different host matrices.

host	device	d_{Al} coverage [a] (nm)	g_{PL} (σ_d)		g_{EL} (σ_d)	
			595 nm ($^5D_0 \rightarrow {}^7F_1$)	612 nm ($^5D_0 \rightarrow {}^7F_2$)	595 nm ($^5D_0 \rightarrow {}^7F_1$)	612 nm ($^5D_0 \rightarrow {}^7F_2$)
solution ($CHCl_3$)	/	none	-1.35±0.09	+0.15±0.02	/	/
PMMA	/	none	-1.35±0.10	+0.13±0.02	/	/
PVK:OXD7 {Zinna, 2015 #11}	/	none	-1.30±0.13	+0.20±0.02	/	/
PVK:OXD7 {Zinna, 2015 #11}	state-of-the-art	6	/	/	-0.79±0.02	+0.15±0.06
TCTA:OXD7	/	none	-1.21±0.02	+0.16±0.02	/	/
TCTA:OXD7	A	6	/	/	-1.00±0.08	+0.19±0.08
TCTA:OXD7	B	20	/	/	-0.21±0.06	+0.03±0.01
TCTA:OXD7	C	110	-0.11±0.01	+0.01±0.01	-0.15±0.06	+0.03±0.01
TCTA:OXD7	D	6	/	/	-0.61±0.14	+0.07±0.04
TCTA:OXD7	E	6	/	/	-0.88±0.14	+0.14±0.09

[a] in addition to 4 nm Ba layer

As expected, the EQE, measured in the forward (fw) direction, through the glass substrate, increases progressively along with the increase of cathode thickness (inset of Figure 3d) up to the maximum value of $5x10^{-3}$ % for device C, thanks to the more efficient extraction of photons from the glass side. Because of the structured emission spectrum of Eu^{3+}, the EQE refers to the integral of several bands, with a dominant contribution from the 612-nm one. The relative weight of each band to total luminescence, remains however constant in all the devices because it only depends on the nature of the emitter, i.e. CsEu(hfbc)$_4$. As a consequence, the comparison in terms of EQE within all the devices discussed in the following and with our previous state of the art device is fully consistent. The rather low values of EQE, comparable to the earlier achievements, impose the search of new approaches for enhanced efficiencies in order to validate CP-OLED technology in lab (next readiness level or TRL 4). Moreover, although the effect of cathode transparency is established, the gap between g_{EL} (~1 at 595 nm) in the prototype with respect to g_{PL} (~1.21 at 595 nm) is still significant, therefore other factors affecting CP EL must be still identified.

We should point out that while reflection has a significant effect in our devices [Zinna, Adv Mat] and in some other ones [Meijers *J. Am. Chem. Soc.* **1997,** *119,* 9909], in other cases [Oda et al, Adv. Mater. 2000, 12, 362. Geng et al, J. Am. Chem. Soc. 2003, 125, 14032. Brandt et al J. Am. Chem. Soc., 2016, 138 (31), pp 9743] this issue was not affecting the polarization performances of the devices. Although the reasons for such differences are not clear, we may consider that different materials used to manufacture the cathodes can partially account for some of the different behaviors observed. Moreover various physical phenomena are involved in a CP-OLEDs, such as scattering, internal reflections and waveguiding effects which in turn may depend on the position of the recombination zone, these factors can vary significantly in devices with different architectures or made with different materials. Unfortunately, to date no comprehensive model explaining the variation of g_{EL} in a device as a function of these parameters have been developed.

In the following we analyze how the position and width of the recombination zone (RZ) of radiative excitons, allied with reflection on the cathode, might affect the polarization of the light collected at the anode. This aspect was neglected in the simplified model that we developed earlier{Zinna, 2015 #11} for proof-of-concept CP-OLEDs. To clarify the effects of RZ position and propose a more accurate model able to describe the g_{EL} trend, we fabricated CP-OLEDs with different positions of the RZ.

Firstly we manufactured and characterized a single layer CP-OLEDs with the same architecture as device A but with the blend TCTA:CsEu(*(–)*-hfbc)$_4$ as the active layer, which features unbalanced charge carrier transport. In this configuration, due to the prevalent hole transporting character of the active layer, the RZ is expected close to the cathode interface and we observed a reduction in g_{EL} value to -0.6 at 595 nm with a very poor EQE.

On the other hand, the use of interfacial layers (ILs) is not only an effective way to improve device performances but also allows one to control the position of the RZ. The IL approach

was developed in OLED technology to control charge carrier injection and blocking, hence providing the exciton confinement within the emissive layer and boost the performance. Since it requires to deposit an additional layer, for several years this technique was only used in vacuum deposited OLEDs. Recently, by keeping the solution process method, semiconducting IL was developed to fabricate a multi-layered OLED architectures. In fact, besides cross-linkable materials, IL compounds with solubility in orthogonal solvents with respect to the active layer can be selected, hence the successive solution deposition of the functional layers becomes possible. The performance of IL-optimized solution processed devices are largely improved in terms of EQE, with a lower turn-on voltage that reduces electrical stress {Hu, 2015 #53}.

The multi-layered approach is totally unexplored in CP-OLEDs technology. Here we fabricate two different architectures, by inserting an IL either at the anode (AIL) or at the cathode (CIL), as shown in Figure 3a for devices D and E, respectively. Beside the possible efficiency enhancement, these architecture would allow us to move the position of RZ close to the cathode or to the anode interfaces hence facilitating the analysis of the effects on g_{EL}.

In the first device architecture (device D), a RZ close to the cathode is obtained by inserting a thin film of hole transporting PVK as the anode IL (AIL, Figure 1) onto the ITO/PEDOT:PSS glass substrate. The 30 nm thick PVK film, deposited from chlorobenzene solution by following the protocol developed earlier {Giovanella, 2011 #42}, is optimal for OLED performance. Moreover, the PVK film is fully transparent to Eu(III) complex emission ($T > 99$ % of 30 nm thick PVK film, Figure S6). The active layer is then deposited from $CHCl_3$ solution and the device is capped with a semitransparent cathode to give the architecture ITO/PEDOT:PSS/AIL/TCTA:OXD7:CsEu(*(–)*-hfbc)$_4$/Ba/Al. The introduction of the PVK layer with a suitable HOMO energy level ($HOMO_{PVK}$ = -5.44 eV, Figure 3b) mitigates the potential energy barrier (~0.7 eV) for hole injection into the active layer ($TCTA_{HOMO}$ ~5.7 eV) at the PEDOT:PSS/active layer interface. The facilitated hole injection,

combined to the higher hole mobility of TCTA than electron mobility of OXD7, most likely shifts the RZ towards the cathode interface. For this device, we observed the reduction of g_{EL} values down to -0.61±0.14 at 595 nm and 0.07±0.04 at 612 nm, and a low fw-EQE ($2x10^{-3}$ %). The device with RZ close to the anode (device E) is obtained by insertion of a cathode IL (CIL) on top of the active layer prior to the metallic cathode deposition. The CIL consists of the alcohol soluble polar polymer Poly[(2,7-(9,9'-dioctyl)fluorene)-alt-(2,7-(9,9'-bis(5"-polyethylene oxide) pentyl)fluorene)] (PolarP, Figure 1), that showed quite considerable benefits for solution processed LEDs {Castelli, 2015 #36}. Thanks to the formation of an electrical dipole at the interface, the CIL promotes the injection of electrons into the active layer and, as a consequence, the RZ is expected to be displaced far from the cathode (i.e. closer to the anode). Besides, the ITO/PEDOT:PSS/TCTA:OXD7:CsEu(*(–)*-hfbc)$_4$/CIL/Ba/Al, with semitransparent cathode, exhibits an enhanced fw-EQE up to 0.05 %, ten times higher than the control device A. The light switches on at 6 V (it was 9 V without CIL, Figure S7) displaying the typical pure Eu-complex EL spectrum. The g_{EL} values of -0.88±0.14 and 0.14±0.09 at 595 nm and 612 nm respectively along with the increased efficiency are very significant with respect to the state-of-the-art {Zinna, 2015 #11;Yang, 2013 #10} although g_{EL} is slightly lower than in the control device A.

All these observations clearly show that the IL has a remarkable effect on the g_{EL} which, to a first understanding, should depend only on the intrinsic property of the emitter combined to the detrimental effect of back electrode (cathode) reflection, as described by a mathematical model we put forward in our previous work {Zinna, 2015 #11}.

In that model, we completely neglected any additional depolarization process within the device, eventually due to scattering, interlayer reflections etc. Indeed, in more complete view, we should consider that, on its travel to the transparent anode, light is attenuated by scattering and absorption processes in the various layers it goes through, which can be conveniently expressed by the transmittance. By itself, this attenuation has minor effect on light

polarization {Li, 2015 #324}, but it changes the relative proportion of light directly emitted forward and light emitted backwards, that reaches the anode only after reflection on the cathode (**Figure 4**). For this reason, the geometrical location of RZ might play a major role.

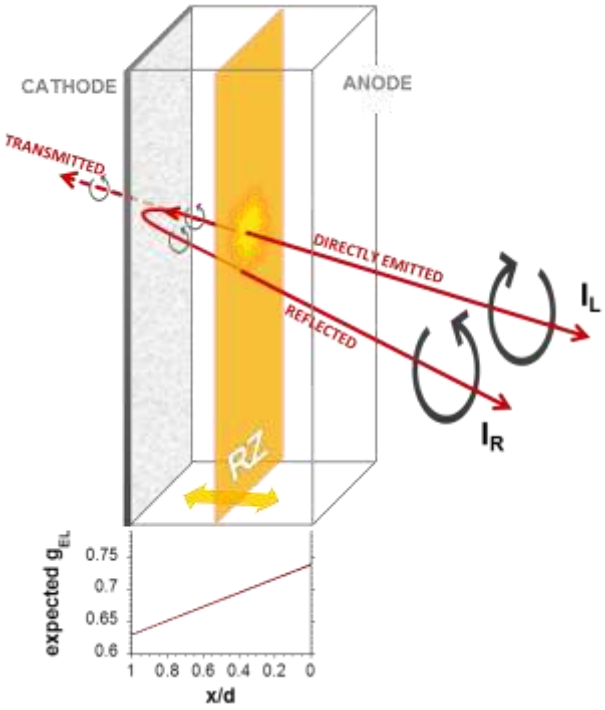

Figure 4. Schematic view of a CP-OLED to illustrate the collection of left- and right-handed CP light. The RZ is represented as an orange thin plane at a distance x from the anode. Curved arrows represent left- and right-handed light polarization: forward and backward direct emitted and reflected light. The loss of degree of circular polarization expected by the model with respect to normalized position of RZ is shown, calculated according to equation 1 with reasonable values for semitransparent device: $g_{EL}^{(0)} = 1.38$, $t_0 = 0.9$, $R = 0.38$.

We assume that excitons are mainly generated in the host and successively transferred, through the FRET mechanism discussed above (Figure 2c), to the CsEu((*–*)-hfbc)$_4$ complex, even if the contribution from direct charge trapping at the chiral emitter sites can not be excluded. We consider that half of the light is emitted forward and half is emitted backward. The light emitted forward is attenuated by a factor depending on T of the active layer itself and of the front layers (PEDOT:PSS, PVK), between RZ and glass. On the contrary, the light emitted backward, attenuated during its travel from the RZ to the cathode, is reflected and changes its handedness. This component reaches the anode undergoing a further attenuation. **Equation 1** (see ESI for the full derivation) is proposed to describe g_{EL} behavior with respect

to RZ position and takes into account the two polarized components I_L' (left) and I_R' (right) actually collected at the glass side:

$$g_{EL} = 2\,\frac{I_L' - I_R'}{I_L' + I_R'} = g_{EL} = g_{EL}^{(0)}\,\frac{1 - R\cdot e^{-2\alpha(d-x)}}{1 + R\cdot e^{-2\alpha(d-x)}} \qquad (1)$$

where $g_{EL}^{(0)}$ is the intrinsic dissymmetry factor of the chiral europium complex, R is the reflectivity of the cathode, t_0 is the attenuation factor taking into account light loss between the electrodes, x is the distance of the RZ from the anode (x=0 on the anode, x=d on the cathode, see Figure S10).

Equation 1 (plotted in Figure 4 with reasonable values of R and t_0 for the device A) suggests that a RZ as close as possible to the anode is optimal to preserve the polarization of emitted light. In fact, in this case, the attenuation of the backward emitted component (which undergoes reflection) is maximal, while the attenuation of the forward emitted component (which exits the anode window without significant polarization loss) is minimized. In the presented devices with semitransparent cathode, the g_{EL} values can vary as much as 15-20% as an effect of only the RZ position (roughly from ≈ 0.63 to ≈ 0.74). These figures are consistent with our experimental observations (see Table 1).

Despite the simplicity of the model and its heuristic nature, it allows us to predict the reduction of g_{EL} values as a function of both the position of the RZ and the reflection of the cathode. However, it should be stressed that this model does not take into account edge effects and multiple internal reflection which may eventually cause additional loss of polarization.

3. Conclusion

In conclusion, we have shown that by a rational design of CP-OLEDs, it is possible to improve both efficiency of the device and polarization of emitted light. The success of our

strategy relies on the use of an intrinsic chiral emitter (i.e. lanthanide complex) in a solution processed multilayered OLED architecture. We attained the highest g_{EL} value (1.0) reported so far for CP-OLEDs which is about 3 times higher than the results commonly achieved by following other approaches (i.e. those based on polymeric emitters). The external quantum efficiency of the present CP-OLEDs is enhanced of one order of magnitude with respect to our proof-of-concept device thanks to the insertion of interfacial layers that regulate charge carrier injection and recombination zone position. We have shown, for the first time, that, beside the critical reflection on the cathode electrode, the position of the recombination zone of radiative polarized excitons, as well as the active layers transmittance may heavily affect the polarization performance. In order to rationalize these outcomes and to be able to bring chiral photonic organic devices to the next TRL, we have put forward a simple model taking into account these effects.

4. Experimental Section

Materials: The CsEu(hfbc)4 complex was synthesized following the procedure reported earlier.{Zinna, 2015 #11} The Polyvinylcarbazole was purchased from Sigma-Aldrich and used as received. The TCTA was was purchased from Sigma-Aldrich and used as received. The OXD7 was purchased from Lumtec. Poly[(2,7-(9,9'-dioctyl)fluorene)-alt-(2,7-(9,9'-bis(5"-polyethylene oxide) pentyl)fluorene)] was synthesized by following the procedure reported earlier.{Castelli, 2015 #36}

Methods: The instrumental set-up for detection of circular polarization of emitted light consisted in a modified NanoLog-TCSPC by Horiba Italia S.r.l. Between the sample and the detector we put a quarter wave plate (Thorlabs, AQWP05M-600) which was rotated through angles defining the orientation of the easy axis vs. the linear polarizer (Oriel 25010), which was kept fix. For the fabrication of CP-OLEDs, glass substrates (25×25×1.1 cm^3) coated with

ITO (sheet resistance 15 □/sq). A 50 nm thick PEDOT:PSS (Clevios) film was spin coated in air over the ITO and thermally annealed at 150 °C inside N_2 filled glove-box for 10 minutes. The high temperature annealing yields a compact hole-conducting layer. The optimal active layer (75 nm) was deposited from 15 mg/ml $CHCl_3$ solution by spincoating at 2000 rpm. Different thickness can be achieved by increasing/decreasing solution concentration. In device B, a thin (30 nm) polyvinylcarbazole (PVK) hole-transport layer was spin-coated from chlorobenzene solution. In device C, a thin layer (~20 nm) PolarP was spincoated from EtOH solution. Cathode consisting of a 4 nm Ba layer coated with 6, 20, 100 nm Al capping layer was finally thermally evaporated in high vacuum ($5 \cdot 10^{-7}$ bar). A Keithley 2602 source meter was used to measure the current−voltage-luminance characteristics of the devices. The light output was measured by a 1 cm^2-sized calibrated silicon photodetector positioned in contact with ITO glass side of the device. The CP-OLED brightness was determined from the fraction of light that reaches the photodetector. CP-OLEDs were tested in nitrogen atmosphere without additional environmental protection. Devices active area is 5 mm^2.

UV-Vis spectra were recorded with a … spectrophotometer, ECD spectra were recorded with a JASCO J-710 spectropolarimeter. In order to check that no significant contributions from linear dichroism/linear birifringence were present, different spectra acquired rotating the samples by 90° and 180° were compared, the same spectra were recorded on both the faces.

PL and PEL…
Transmittance…
Cyclic voltammetry…
Phoshorescence spectrum…

Supporting Information
Supporting Information is available from the Wiley Online Library.

Acknowledgements

Financial support from MIUR-PRIN 2012A4Z2RY, Cariplo Foundation (2012-0844), and University of Pisa (PRA 2016-50 “Materiali Funzionali”) is acknowledged.

Received: ((will be filled in by the editorial staff))
Revised: ((will be filled in by the editorial staff))
Published online: ((will be filled in by the editorial staff))

The table of contents entry should be 50–60 words long, and the first phrase should be bold. The entry should be written in the present tense and impersonal style. The text should be different from the abstract text.

Keyword

C. Author 2, D. E. F. Author 3, A. B. Corresponding Author* ((same order as byline))

Title ((no stars))

ToC figure ((Please choose one size: 55 mm broad × 50 mm high **or** 110 mm broad × 20 mm high. Please do not use any other dimensions))

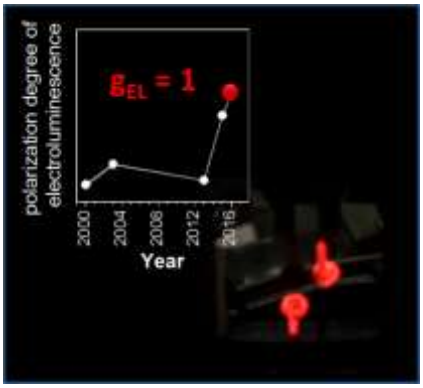

Supporting Information

Design of lanthanide-based OLEDs with remarkable circularly polarized electroluminescence

Francesco Zinna[a], Mariacecilia Pasini[b], Francesco Galeotti[b], Chiara Botta[b], Lorenzo Di Bari[a,] and Umberto Giovanella[b,]**

Experimental details

Photophyisical data

Table S1. Photophyisical parameters of Eu-complexes in solution. Eu(TTA)Phen is included for…

emitter	PL-QY (%)	τ_{obs} (μs)	$PL\text{-}QY_{intr}$	η_{sens} (%)
CsEu(*(-)*-hfbc)$_4$	3.5	150	0.09	16.3
Eu(TTA)Phen[S1]	48	710	0.51	95

According to the common procedure,[S2] the triplet level of CsEu((−)-hfbc)$_4$ was determined by measuring the phosphorescence of the isostructural complex[S3] CsGd((−)-hfbc)$_4$ (Figure S2). In fact, unlike Eu^{3+}, Gd^{3+} ion has no level able to accept energy from the ligand triplet level and so no Ln-centred emission can be observed. The spectrum was measured in a CH_2Cl_2 (degassed) frozen solution (C =...) at 77 K.

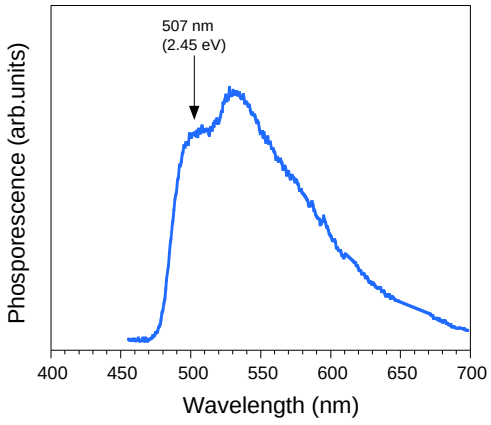

Figure S2. Phosphorescence of CsGd(*(–)*-hfbc)$_4$ frozen solution.

Table S2. HOMO, LUMO, energy levels and charge carrier mobility of host materials.

Compounds	HOMO (eV)	LUMO (eV)	triplet energy $T_1 \rightarrow S_0$ (eV)	Charge carrier Mobility (cm^2/Vs) h	e	REF.
TCTA	-5.7	-2.3	2.8	~10^{-4}	/	[S4, S5]
OXD7	-6.2	-2.6	/	/	~10^{-5}	[S6]

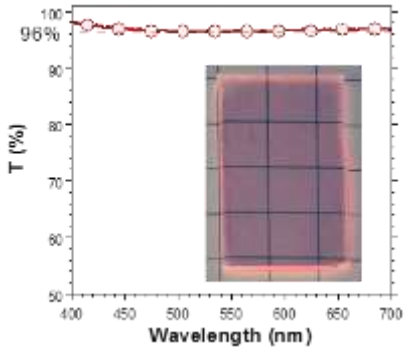

Figure S3. Transmittance of TCTA:OXD7:12wt.% CsEu((–)-hfbc)$_4$ film on glass; inset, image of the film under UV light.

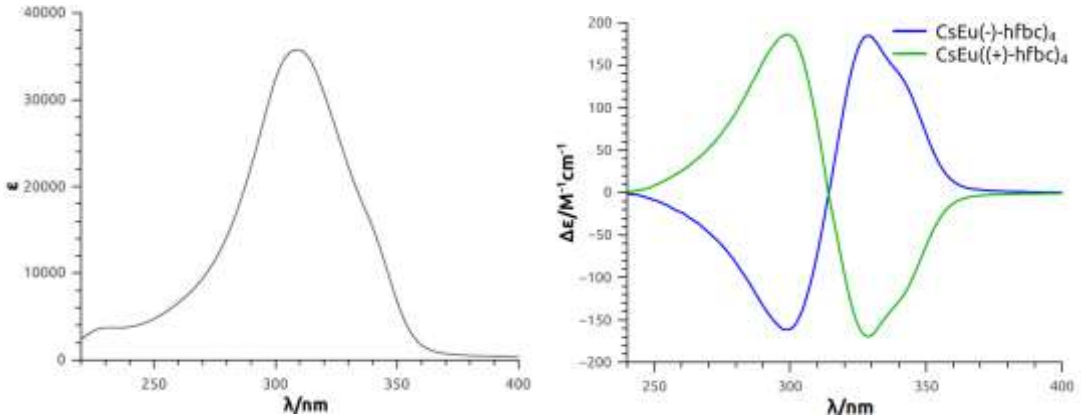

Figure S4. Absorption (a) and ECD (b) for CsEu(hfbc)$_4$ in $CHCl_3$ solution.

Single layer CP-OLEDs with different active layer thickness were fabricated. Due to the pretty high operational voltage of semitransparent devices without CIL (> 15−18 V) , the thickness of the active layer cannot be increased above ~100 nm to maintain good reproducibility of the performance. The thickness had no effect on g_{PL} of uncovered films (−1.21 ± 0.02 at 595 nm for both 75 and 100 nm films) while a reduction of g_{EL} was observed as the thickness increased. Besides the highest $g_{EL} = 1$ for ~75 nm thick device A, values

of -0.95 and 0.11 at 595 and 612 nm respectively for ~80 nm thick device, and -0.8 and 0.04 at 595 and 612 nm respectively for ~95 nm thick active layer device were measured.

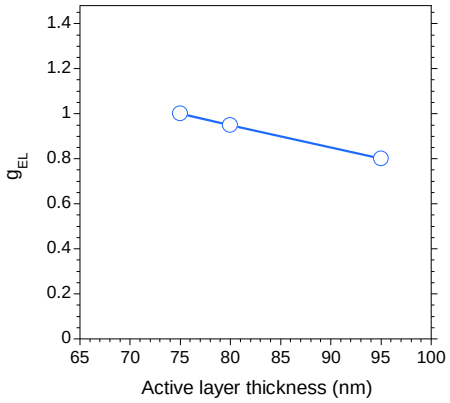

Figure S5. g_{EL} behavior *vs* active layer thickness.

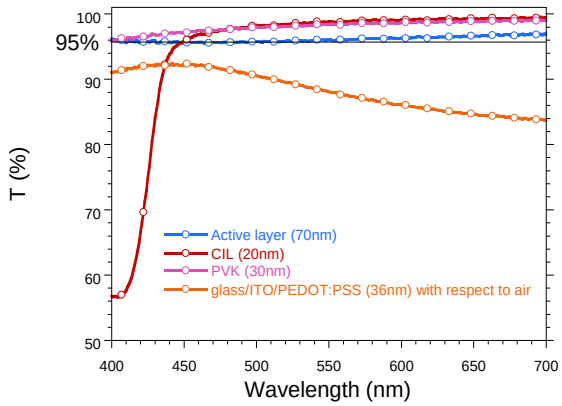

Figure S6. Transmittance spectra of the various layers of the device

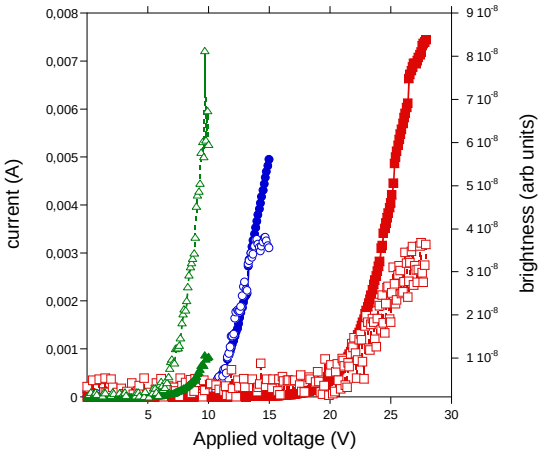

Figure S7. Representative current (filled symbols)-brightness (empty symbols)-voltage characteristics of ITO/PEDOT/ TCTA:OXD7:12wt.% CsEu(*(–)*-hfbc)$_4$ /Ba/Al (blue), ITO/PEDOT/AIL/ TCTA:OXD7:12wt.% CsEu(*(–)*-hfbc)$_4$ /Ba/Al (red) and ITO/PEDOT/ TCTA:OXD7:12wt.% CsEu(*(–)*-hfbc)$_4$/CIL/Ba/Al (green) devices with semitransparent cathode.

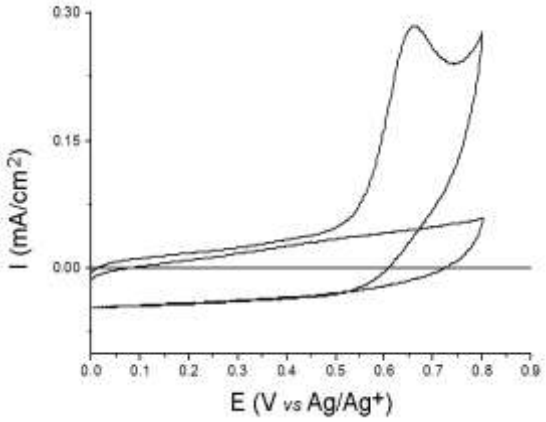

Figure S8. Cyclic voltammograms of the complexes CsEu(*(–)*-hfbc)$_4$ recorded vs Ag/Ag+ in acetonitrile at 298 K (scan rate: 100 mV s^{-1}), TBAP, CG 0.06 cm^2.

Effects of the electrodes-recombination zone (RZ) position on the polarization efficiency.
As in our previous model,[S7] we consider that half of the radiation is emitted forward and half backward. According to Beer–Lambert law, the emitted light (I_0) is attenuated exponentially with the distance x (see Figure S10) between the anode and the recombination zone, where the photon is generated:

$$I = I_0 e^{-\alpha x} \qquad \text{(eq. S1)}$$

where In first approximation, we shall consider that the light is emitted only by an infinitesimally thin layer of the active layer (see Figure S9). The loss of the fraction of the light emitted forward is described by equation S1. The loss of the fraction of the light emitted backward varies with the distance of the recombination zone from the cathode. This component eventually undergoes reflection on the cathode, and therefore its handedness is reversed.
The pathway traveled by the backward light is conveniently divided into three steps:

- In the way between the RZ and the cathode, it is attenuated by a factor $e^{-\alpha(d-x)}$.
- Owing to the reflection on the cathode surface it is further attenuated by a factor R (reflectance) and its handedness is reversed.
- In the way back from the cathode to the anode, it is finally attenuated by a factor $e^{-\alpha d}$

The total attenuation factor is therefore:

Applying these attenuation factors to the two polarized component ($I_L^{(0)}$ and $I_R^{(0)}$) and taking into account the sign reversal of the polarization after reflection, we have that the two polarized components exiting the device (I_L' and I_R') are:

$$I_L' = \frac{1}{2} I_L^{(0)} \cdot e^{-\alpha x} + \frac{1}{2} I_R^{(0)} \cdot R \cdot e^{-\alpha(2d-x)} \qquad \text{(eq. S2a)}$$

$$I_R' = \frac{1}{2} I_R^{(0)} \cdot e^{-\alpha x} + \frac{1}{2} I_L^{(0)} \cdot R \cdot e^{-\alpha(2d-x)} \qquad \text{(eq. S2b)}$$

Where $I_L^{(0)}$ and $I_R^{(0)}$ are the intrinsic polarization components emitted by the chiral molecule.

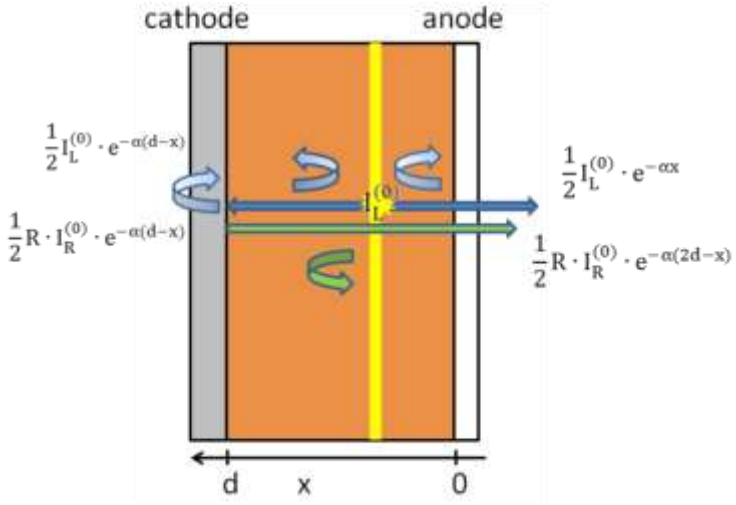

Figure S9: Schematic representation of a device. The yellow strip represents the recombination zone, curved arrows represent light losses. Light before reflection is indicated in blue, light after reflection is indicated in green. On top of each arrow, we report the attenuation for the left polarized component.

The overall g_{EL} factor that we measure for the device is:

$$g_{EL} = 2\frac{I_L' - I_R'}{I_L' + I_R'} \qquad \text{(eq. S3)}$$

By substituting eq. (S2a) and (S2b) in eq. (S3) and rearranging the terms, we obtain:

$$g_{EL} = 2\frac{e^{-\alpha x}\left(I_L^{(0)} - I_R^{(0)}\right) - R \cdot e^{-\alpha(2d-x)}\left(I_L^{(0)} - I_R^{(0)}\right)}{e^{-\alpha x}\left(I_L^{(0)} + I_R^{(0)}\right) + R \cdot e^{-\alpha(2d-x)}\left(I_L^{(0)} + I_R^{(0)}\right)} = 2\frac{\left(I_L^{(0)} - I_R^{(0)}\right)}{\left(I_L^{(0)} + I_R^{(0)}\right)} \cdot \frac{e^{-\alpha x} - R \cdot e^{-\alpha(2d-x)}}{e^{-\alpha x} + R \cdot e^{-\alpha(2d-x)}} \qquad \text{(eq. S4)}$$

We note that $2\frac{\left(I_L^{(0)} - I_R^{(0)}\right)}{\left(I_L^{(0)} + I_R^{(0)}\right)} = g_{EL}^{(0)}$, i.e. the intrinsic g factor of the chiral emitter, and by substituting it in eq. (S4), after multiplying by $e^{+\alpha x}$ both the numerator and denominator, we get:

$$g_{EL} = g_{EL}^{(0)} \frac{1-R\cdot e^{-2\alpha(d-x)}}{1+R\cdot e^{-2\alpha(d-x)}} \quad \text{(eq. 1)}$$

where $g_{EL}^{(0)}$ is the intrinsic dissymmetry factor of the chiral europium complex. Eq. (1) shows that g_{EL} monotonously increases with x, meaning that higher g_{EL}-s are expected when the recombination zone is close to the anode interface.
It is worth noting that when the recombination occurs very close to the anode (x = 0), eq. (1) becomes:

$$g_{EL} = g_{EL}^{(0)} \frac{1-R\cdot e^{-2\alpha d}}{1+R\cdot e^{-2\alpha d}} \quad \text{(eq. S5)}$$

Since $e^{-\alpha d} = T$, i.e. the overall transmittance of the active layer and the CIL, eq. (S5) becomes:

$$g_{EL} = g_{EL}^{(0)} \frac{1-R\cdot T^2}{1+R\cdot T^2} \quad \text{(eq. S6)}$$

In the opposite case, when the recombination occurs very close to the cathode (x = d), we have:

$$g_{EL} = g_{EL}^{(0)} \frac{1-R}{1+R} \quad \text{(eq. S7)}$$

Equation S7 is the equation worked out in our previous model, which did not take into account loss of radiation within the layers between anode and cathode.
Plotting eq. (1) with reasonable values for semitransparent device ($g_{EL}^{(0)} = 1.38$, $T = 0.9$, $R = 0.38$, for a 6 nm Al cathode[S7]), the g_{EL} can vary as much as 15-20 % as an effect only of the recombination zone position (roughly from ≈0.6 to ≈0.7). For the sake of comparison, in Table S3 we show the experimental g_{EL} values obtained for different architecture sorted by RZ position.

Table S3. Experimental g_{EL} values obtained for different architecture sorted by RZ position and expected g_{EL} in the two limit cases as predicted by eq. (S6) and eq. (S7).

RZ near to the	device[a]	Experimental g_{EL}	Calculated g_{EL}
cathode	AIL/TCTA:OXD7	0.61	0.63
	AIL/TCTA	0.6	
anode	TCTA:OXD7/CIL	0.88	0.74
	TCTA:OXD7	1/0.8[b]	

[a] semitransparent cathode; [b] 100 nm active layer thickness

However, when the recombination zone can not be approximated to be reasonably thin with respect to the active layer thickness,[S8] eq. (1) should be integrated over the whole active layer, after being weighted with a function $\rho = \rho(x)$ describing the spatial distribution of the recombination zone:

$$g_{EL} = \int_0^d g_{EL}^{(0)} \frac{1-R\cdot e^{-2\alpha(d-x)}}{1+R\cdot e^{-2\alpha(d-x)}} \rho(x)\, dx \qquad \text{(eq. S8)}$$

References

[S1] C. Freund, W. Porzio, U. Giovanella, F. Vignali, M. Pasini, S. Destri, A. Mech, S. Di Pietro, L. Di Bari, and P. Mineo, *Inorg. Chem.*, 2011. **50**, 5417.

[S2] K. Binnemans, Coord. Chem. Rev., 2015, **295**, 1.

[S3] S. Di Pietro, L. Di Bari, *Inorg. Chem.*, 2012, **51**, 12007.

[S4] S. Höfle, C. Bernhard, M. Bruns, C. Kübel, T. Scherer, U. Lemmer, and A. Colsmann, *ACS Appl. Mater. Interfaces* 2015, **7**, 20769.

[S5] D. P.-K. Tsang, M.-Y. Chan, A. Y.-Y. Tam, V. W.-W. Yam, *Org. Electron*. 2011, **12**, 1114.

[S6] Y.-T. Chang, J.-K. Chang, Y.-T. Lee, P.-S. Wang, J.-L. Wu, C.-C. Hsu, I-W. Wu, W.-H. Tseng, T.-W. Pi, C.-T.Chen, and C.-I Wu, *ACS Appl. Mater. Interfaces* 2013, **5**, 10614.

[S7] F G. Hass, J. E. Waylonis, *J. Opt. Soc. Am*.1961, **51**, 719.

[S8] N. C. Erickson, and R. J. Holmes, *Adv. Funct. Mater.* 2013, **23**, 5190.